Simulation studies of the $Cl^- + CH_3I$ S_N2 nucleophilic substitution reaction: Comparison with ion imaging experiments

Jiaxu Zhang, Upakarasamy Lourderaj, Rui Sun, Jochen Mikosch, Roland Wester' , and William L. Hase'

Citation: J. Chem. Phys. **138**, 114309 (2013); doi: 10.1063/1.4795495
View online: http://dx.doi.org/10.1063/1.4795495
View Table of Contents: http://aip.scitation.org/toc/jcp/138/11
Published by the American Institute of Physics

RIGHTSLINK

THE JOURNAL OF CHEMICAL PHYSICS **138**, 114309 (2013)

Simulation studies of the $Cl^- + CH_3I$ S_N2 nucleophilic substitution reaction: Comparison with ion imaging experiments

Jiaxu Zhang,[1] Upakarasamy Lourderaj,[2] Rui Sun,[2] Jochen Mikosch,[3] Roland Wester,[4,a)] and William L. Hase[2,a)]

[1]*Beijing National Laboratory for Molecular Sciences, State Key Laboratory of Molecular Reaction Dynamics, Institute of Chemistry, Chinese Academy of Sciences, Beijing 100190, China*
[2]*Department of Chemistry and Biochemistry, Texas Tech University, Lubbock, Texas 79409-1061, USA*
[3]*National Research Council of Canada, Steacie Institute for Molecular Sciences, 100 Sussex Drive, Ottawa, Ontario K1AOR6, Canada*
[4]*Institut fur Ionenphysik und Angewandte Physik, Universität Innsbruck, Technikerstraße 25/3, A-6020 Innsbruck, Austria*

(Received 2 September 2012; accepted 28 February 2013; published online 21 March 2013)

In the previous work of Mikosch *et al*. [Science **319**, 183 (2008)], ion imaging experiments were used to study the $Cl^- + CH_3I \rightarrow ClCH_3 + I^-$ reaction at collision energies E_{rel} of 0.39, 0.76, 1.07, and 1.9 eV. For the work reported here MP2(fc)/ECP/d direct dynamics simulations were performed to obtain an atomistic understanding of the experiments. There is good agreement with the experimental product energy and scattering angle distributions for the highest three E_{rel}, and at these energies 80% or more of the reaction is direct, primarily occurring by a rebound mechanism with backward scattering. At 0.76 eV there is a small indirect component, with isotropic scattering, involving formation of the pre- and post-reaction complexes. All of the reaction is direct at 1.07 eV. Increasing E_{rel} to 1.9 eV opens up a new indirect pathway, the roundabout mechanism. The product energy is primarily partitioned into relative translation for the direct reactions, but to CH_3Cl internal energy for the indirect reactions. The roundabout mechanism transfers substantial energy to CH_3Cl rotation. At E_{rel} = 0.39 eV both the experimental product energy partitioning and scattering are statistical, suggesting the reaction is primarily indirect with formation of the pre- and post-reaction complexes. However, neither MP2 nor BhandH/ECP/d simulations agree with experiment and, instead, give reaction dominated by direct processes as found for the higher collision energies. Decreasing the simulation E_{rel} to 0.20 eV results in product energy partitioning and scattering which agree with the 0.39 eV experiment. The sharp transition from a dominant direct to indirect reaction as E_{rel} is lowered from 0.39 to 0.20 eV is striking. The lack of agreement between the simulations and experiment for E_{rel} = 0.39 eV may result from a distribution of collision energies in the experiment and/or a shortcoming in both the MP2 and BhandH simulations. Increasing the reactant rotational temperature from 75 to 300 K for the 1.9 eV collisions, results in more rotational energy in the CH_3Cl product and a larger fraction of roundabout trajectories. Even though a $ClCH_3$–I^- post-reaction complex is not formed and the mechanistic dynamics are not statistical, the roundabout mechanism gives product energy partitioning in approximate agreement with phase space theory. © *2013 American Institute of Physics*. [http://dx.doi.org/10.1063/1.4795495]

I. INTRODUCTION

Studies of $X^- + CH_3Y \rightarrow XCH_3 + Y^-$ S_N2 bimolecular nucleophilic substitution reactions have attracted extensive experimental[1–14] and computational attention.[15–24] These reactions have a potential energy surface with a central barrier $[X–CH_3–Y]^-$ separating the potential energy minima of the X^-–CH_3Y and XCH_3–Y^- complexes, as depicted in Figure 1. This potential model has been confirmed by numerous theoretical and experimental studies.[1–4] Statistical theories such as Rice-Ramsperger-Kassel-Marcus (RRKM),[25] phase space theory (PST),[25] and transition state (TST)[26] theory have been widely used to model the kinetics of S_N2 reactions. However, the results of many experimental studies of S_N2 reactions are not adequately explained by these theories.[5–15] Chemical dynamics simulations[16–24] have proven very useful for interpreting the kinetics and dynamics of S_N2 reactions, and have brought into question fundamental assumptions of statistical theories regarding mode specific chemistry, intramolecular vibrational energy redistribution (IVR), the dynamics of central barrier crossing, and the efficiency of ion-molecule capture.

Recently, Wester and co-workers reported kinematically complete reactive scattering experiments of the S_N2 reactions $X^- + CH_3I \rightarrow XCH_3 + I^-$ (X = F and Cl) using the ion-molecule crossed beam imaging spectrometer, with well defined relative kinetic energy and momentum,[27,28] and the results for $Cl^- + CH_3I$ are summarized in Figure 2. They measured directly the velocity vector of the product anion which reveals the energy- and angle-differential reaction cross

a)Electronic addresses: bill.hase@ttu.edu and roland.wester@uibk.ac.at

 © 2013 American Institute of Physics

RIGHTSLINK

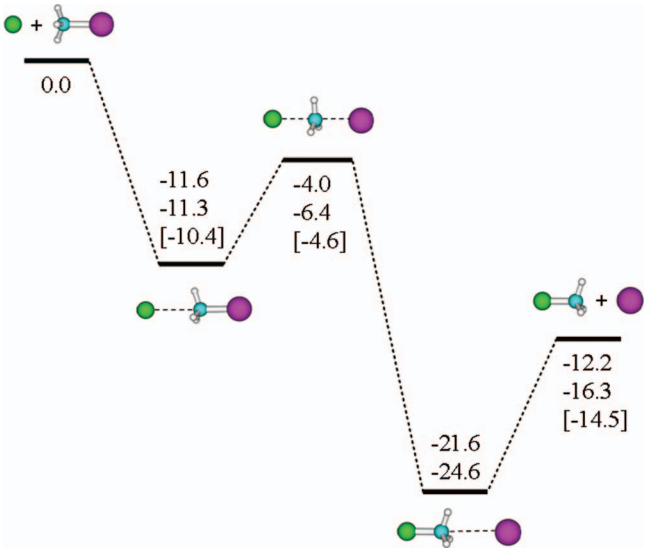

FIG. 1. Potential energy curve for the $Cl^- + CH_3I \rightarrow CH_3Cl + I^-$ S_N2 reaction. The upper and lower energies are the MP2(fc)/ECP/d and BhandH/ECP/d values, respectively. The energies are in kcal/mol and at 0 K, and do not include ZPEs. The energies in brackets are the experimental values. The experimental Cl^-–CH_3I complexation energy is the enthalpy at 298 K from Ref. 11. The experimental barrier is the 0 K barrier, with ZPE included, obtained by fitting the reaction rate constant with an ion-molecule capture statistical model; from Ref. 7. The experimental 0 K reaction exothermicity, without ZPE included, is determined using standard molar enthalpies of formation in Ref. 63 and harmonic frequencies in Ref. 64.

section. The manner in which the total available energy is partitioned to internal degrees of freedom of the molecular product and to product relative translation may be determined from the experiments. Chemical dynamics simulations[29] provide a means to establish an atomic-level understanding of these experimental product energy and angular distributions.

Direct dynamics simulations, for which classical trajectories are directly coupled with electronic structure theory,[21–23,30] reproduce the product energy partitioning and velocity scattering angle distributions measured in experiments for the highly exothermic $F^- + CH_3I \rightarrow FCH_3 + I^-$ reaction.[31] At the same time, the simulations reveal that the substitution reaction occurs by two direct atomic-level mechanisms, i.e., rebound and stripping, and an indirect mechanism, proceeding via a F^-–HCH_2I hydrogen-bonded complex.

In the previous work,[27] the results of ion imaging experiments and direct dynamics simulations were used to study the $Cl^- + CH_3I \rightarrow ClCH_3 + I^-$ S_N2 reaction at the high collision energy of 1.9 eV. The results of the simulations agree with the product energy partitioning and velocity scattering angle distributions measured experimentally. The experimental distributions suggest the reaction occurs by two different atomistic mechanisms and this is confirmed by the simulations. The latter show that the dominant mechanism is a direct substitution in which Cl^- collides with the backside of CH_3I. The simulations reveal that the second mechanism, resulting in a statistical-like energy partitioning to the products, is a previously unknown mechanism involving CH_3 rotation and called the *roundabout* mechanism.[27]

In the work presented here, direct dynamics simulations[21–23,30] for the $Cl^- + CH_3I \rightarrow ClCH_3 + I^-$ S_N2 reaction are extended to the lower collision energies of 0.39, 0.76, and 1.07 eV, which have also been studied

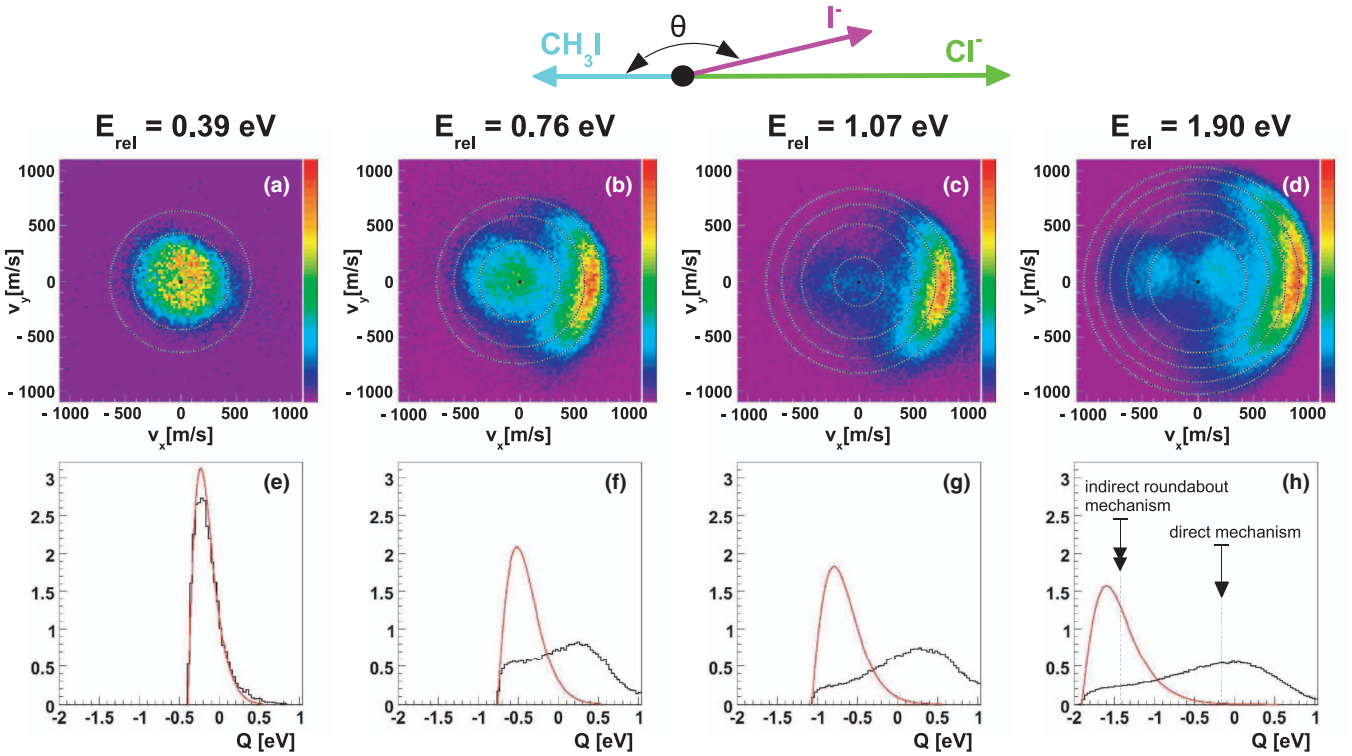

FIG. 2. (a)–(d) Center-of-mass images of the I^- reaction product velocity from the reaction of Cl^- with CH_3I at four different relative collision energies. The image intensity is proportional to $[(d^3\sigma)/(dv_x\, dv_y\, dv_z)]$: Isotropic scattering results in homogeneous ion distribution on the dector. (e)–(h) The energy transfer distributions extracted from the images in (a)–(d) in comparison with phase space theory calculation (red curve). The arrows in (h) indicate the average Q value obtained from the direct chemical dynamics simulations. Adapted from Ref. 27 with permission.

RIGHTSLINK

experimentally.[27] The goal is to obtain an atomic-level understanding of the reaction mechanisms and dynamics for the $Cl^- + CH_3I \rightarrow ClCH_3 + I^-$ reaction for the broad 0.39–1.9 eV range of collision energies. The accuracy of the simulations may be tested by comparing with the ion imaging measurements of Wester and co-workers.[27,28] It is expected that this study will provide a deeper understanding of the atomistic dynamics of gas-phase S_N2 reactions as well as for other complex ion-molecule reactions.

II. COMPUTATIONAL PROCEDURE

In the previous work,[27] direct chemical dynamics simulations, at the MP2(fc)/ECP/d level of theory, were used to study the dynamics of the $Cl^- + CH_3I$ reaction. Very good agreement with the results of ion imaging experiments was obtained for the 1.9 eV collision energy.[27] Detailed electronic structure calculations, involving comparisons of different theories,[32] show this MP2 (Ref. 33) method gives good stationary point properties for the $Cl^- + CH_3I \rightarrow ClCH_3 + I^-$ potential energy surface (PES). This is illustrated in Figure 1, where comparison is made with experiment. For the ECP/d basis set, the double (d) zeta basis set aug-cc-pVDZ[34] was used for the C, H, and Cl-atoms. For iodine, the Wadt and Hay effective core potential (ECP) was used for the core electrons and an uncontracted 3*s*3*p* basis set for the valence electrons.[35] This iodine basis set was augmented by a *d*-polarization function with a 0.262 exponent, and *s*, *p*, and *d* diffuse functions with exponents of 0.034, 0.039, and 0.0873, respectively.[36] The MP2(fc)/ECP/d method is a practical approach for the direct dynamics simulations[32] and, to retain consistency with the previous simulation,[27] this method is also used here.

To compare with the experiments, the simulations were performed at the collision energies (E_{rel}) of 0.39, 0.76, 1.07, and 1.9 eV and CH_3I vibrational and rotational temperatures of $T_v = 360$ and $T_r = 75$ K, respectively.[27,28] The temperature dependence of the chemical dynamics at E_{rel} of 1.9 eV was investigated by using a 300 K room temperature for CH_3I vibration and rotation in contrast to the above T_v and T_r. As discussed in Secs. III B and III C, the MP2(fc)/ECP/d simulation results at $E_{rel} = 0.39$ eV do not agree with experiment. The experimental E_{rel} values are average values for an indefinite narrow distribution of collision energies. At the lowest E_{rel} of 0.39 eV the width of this distribution is an appreciable fraction of 0.39 eV. To investigate how the reaction dynamics may vary for energies within this distribution, simulations were also performed at the lower E_{rel} of 0.20 eV.

To compare with and confirm the MP2 direct dynamics for the low collision energies of 0.39 and 0.20 eV, simulations for these energies were also performed with the DFT/BhandH/ECP/d level of theory.[37] Extensive work has been done to test the performance of density functional theory (DFT)[38–46] and MP2 (Ref. 36) S_N2 reactions and the studies have shown the propensity of DFT to underestimate S_N2 barriers unless the amount of Hartree-Fock exchange is increased.[39–46] A number of different DFT functionals were compared for the $Cl^- + CH_3I$ S_N2 reaction and the results suggest that BhandH/ECP/d is the preferred DFT method for direct dynamics simulations, since it gives the best agreement with CCSD(T)[47] energies for the reactions's PES.[32] The BhandH/ECP/d and MP2(fc)/ECP/d stationary point energies are compared in Figure 1.

The simulations were performed using a software package consisting of the *VENUS* general chemical dynamics computer program[48,49] interfaced to the *NWChem* electronic structure computer program.[50,51] Standard algorithms were used to select initial conditions for the trajectories.[29] Quasi-classical sampling,[29] which includes zero-point energy, was used to select initial coordinates and momenta for the trajectories. The CH_3I vibrational and rotational degrees of freedom were sampled from their respective T_v and T_r Boltzmann distributions. CH_3I had a random orientation with respect to Cl^- and the $Cl^- + CH_3I$ center-of-mass separation was set at 15 Å, with an initial relative velocity for E_{rel} of 0.20–1.9 eV and the specified collision impact parameter *b*. Each trajectory was integrated for a maximum of ∼12 ps. Integrating one MP2(fc)/ECP/d trajectory for 12 ps required ∼7 days on a 3.0 GHz dual-slot quad-core node with 16 GB RAM. The DFT trajectories are ∼3 times faster than those for MP2 theory and integrating one trajectory with BhandH/ECP/d for ∼12 ps required ∼2.5 days on the same cluster.

III. MP2 TRAJECTORY RESULTS AND DISCUSSIONS

A. Reaction probability and microscopic reaction mechanisms

The reaction dynamics were studied versus impact parameter *b* by calculating numerous trajectories at fixed values of *b*, for $T_v = 360$ and $T_r = 75$ K. The resulting reaction probability $P_r(b)$ versus *b* is plotted in Figure 3 for the different E_{rel}. Even though the reaction has no overall barrier, the simulations show a quite low reaction probability at all collision energies, which decreases as the collision energy is decreased and/or the impact parameter is increased. For E_{rel} of 0.2 and 0.39 eV the respective P_r(b) are approximately 0.01 and 0.02 for $b = 0$. For the $F^- + CH_3I \rightarrow CH_3F + I^-$ S_N2 reaction, accurate values for the limiting impact parameter b_{max} are found by assuming the $F^- + CH_3I$ orbital angular momentum adds to the two largest moment of inertia rotational degrees of freedom giving rise to a centrifugal potential at the central barrier transition state.[52] Applying this model to the $Cl^- + CH_3I$ S_N2 reaction studied here results in estimated values for b_{max} of 6.8, 6.0, 5.5, 5.4, and 5.2 Å for E_{rel} of 0.2, 0.39, 0.76, 1.07,

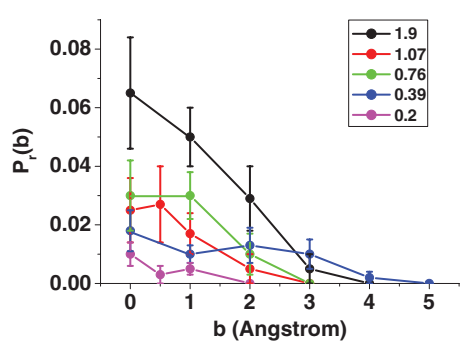

FIG. 3. MP2(fc)/ECP/d reaction probability $P_r(b)$ versus impact parameter *b* for E_{rel} of 0.2–1.9 eV and T_v /T_r = 360 K/75 K.

RIGHTSLINK

and 1.9 eV, respectively. All are greater than 5 Å. However, the low reaction probabilities at large b makes it computationally intractable to sample the complete range of b. To illustrate, no reaction was observed out of 200 trajectories at $b = 4$ Å for the 1.9 eV simulation. For the remaining E_{rel} of 0.2, 0.39, 0.76, and 1.07 eV the respective b and number of trajectories for which no reaction was observed are 2 Å-800, 5 Å-400, 3 Å-200, and 3 Å-200. Though the reaction probability for each E_{rel} cannot be investigated for the expected complete range of b, important details of the reaction dynamics are still obtained.

The simulations revealed that the substitution reaction occurs by two direct atomic-level mechanisms, i.e., rebound and stripping, and several types of indirect mechanisms. These mechanisms were identified by the atomistic motions of the trajectories. The rebound reaction occurs by Cl^- attack of the backside of CH_3I and direct displacement of I^-. The stripping reaction occurs when Cl^- approaches CH_3I on its side and directly strips away the CH_3-group. As discussed in more detail below, the direct rebound mechanism is a small impact parameter process and results in backward scattering. In contrast, stripping occurs for large impact parameters and gives forward scattering. These two direct mechanisms have been observed in previous simulations of the $F^- + CH_3I$ (Ref. 31) and $Cl^- + CH_3Y$ (Y = Cl, Br, I) S_N2 reactions.[24,27,53] The atomistic motions for the rebound and stripping mechanisms are depicted in Figure 3 of Ref. 31.

The indirect reaction occurs by multiple mechanisms including the roundabout,[27] formation of the Cl^-–CH_3I and/or $ClCH_3$–I^- pre- and post-reaction complexes, central barrier recrossing, and coupling of these reaction events. The roundabout mechanism proceeds via one or more CH_3 rotations and an atomistic depiction was given previously.[27] For this mechanism Cl^- first strikes the CH_3 group on its side, causing it to rotate one or more times around the massive I atom. Then, after one or more CH_3 revolutions, Cl^- attacks the C atom backside and directly displaces I^-. Forming the Cl^-–CH_3I or $ClCH_3$–I^- complex means the trajectory becomes temporarily trapped in the pre- or post-reaction potential energy wells (see Figure 1). A trajectory which forms the pre-reaction complex is depicted in Figure 4. Complex formation has been observed previously in simulations of the $Cl^- + CH_3Cl$ (Ref. 17) and $Cl^- + CH_3Br$ (Ref. 24) reactions. Barrier recrossing was observed previously in the central barrier dynamics for $Cl^- + CH_3Cl$.[22,54] Animations of trajectories for the above different mechanisms are presented on the website monte.chem.ttu.edu/group/animations/ch3i.html.

Fractions of the different reaction mechanisms are given in Figure 5 for the five collision energies from 0.2 to 1.9 eV. There are 52, 10, 29, 23, and 5 reactive trajectories with $b > 0$ for E_{rel} of 1.9, 1.07, 0.76, 0.39, and 0.20 eV, respectively, and they are properly weighted by the impact parameters to obtain the fractions in Figure 5. With $b = 0$ included the total number of reactive trajectories for these respective E_{rel} are 63, 15, 35, 30, and 11. As shown in Figure 5, for E_{rel} of 1.9, 1.07, 0.76, and 0.39 eV the atomic-level dynamics are similar, with the direct rebound mechanism dominating with a fraction ranging from 0.73 to unity. The dominant indirect mechanism at E_{rel} of 1.9 eV is the roundabout mechanism with a fraction of

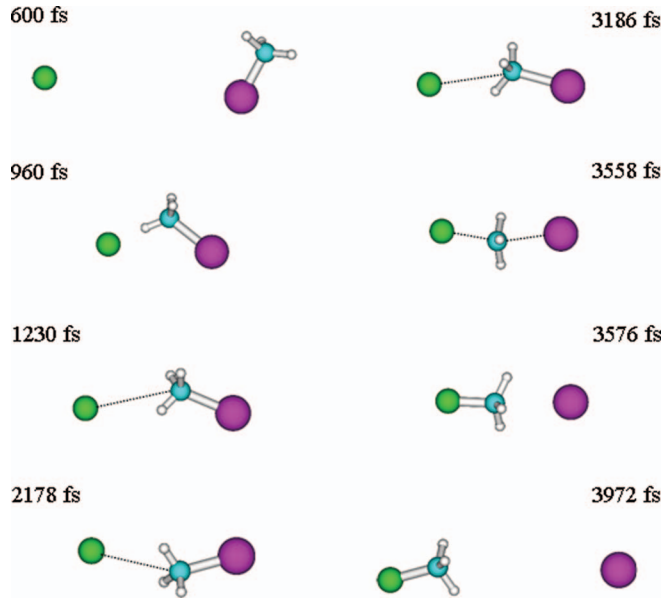

FIG. 4. Atomistic dynamics of a typical trajectory for the indirect reaction mechanism that proceeds via formation of the Cl^-–CH_3I pre-reaction complex.

0.17, which is much higher than for any of the other collision energies. The roundabout mechanism occurs with either one or multiple CH_3 rotations, and with a lifetime between the initial Cl^-–CH_3 collision and the departure of I^- ranging from ~400 fs to 1 ps. More details about the dynamics of crossing the central barrier and energy transfer for the roundabout mechanism are discussed in Sec. V.

For collisions with E_{rel} of 1.07 eV only the direct rebound mechanism was found. At 0.76 eV indirect mechanisms contribute 13% of the chemical reaction. Surprisingly, for the lower collision energy of 0.39 eV the indirect component is even smaller, i.e., 1%, with stripping contributing 11% of the reaction.

There is a dramatic change in the reaction dynamics, from what was found at E_{rel} of 1.9, 1.07, 0.76, and 0.39 eV, when E_{rel} is decreased to 0.20 eV. The direct fraction of the reaction (all rebound) is lowered substantially to only 17%. The vast majority of the reaction, i.e., 83%, now occurs by indirect mechanisms, each involving Cl^-–CH_3I pre-reaction complex formation. There are three indirect mechanisms; i.e., formation of the Cl^-–CH_3I pre-reaction complex alone, coupling of this complex formation with the roundabout mechanism, and forming both the Cl^-–CH_3I and $ClCH_3$–I^- complexes with inclusion of barrier recrossing. These three indirect mechanisms have intermediate lifetimes which range from 2 to 7 ps.

It is noteworthy that the following $b = 0$ results are consistent with the reaction dynamics as described above. There are 4 direct rebound and 7 roundabout trajectories at $E_{rel} = 1.9$ eV. For the above $b > 0$ dynamics direct rebound contributes 17% to the reaction and comparison with these $b = 0$ results indicates that the roundabout mechanism is enhanced by small impact parameters. At $E_{rel} = 1.07$ eV there are 4 direct rebound and 1 roundabout trajectory, consistent with the dominance of the direct rebound mechanism and a sharp transition in the reaction dynamics in going from E_{rel} of 1.9

RIGHTSLINK

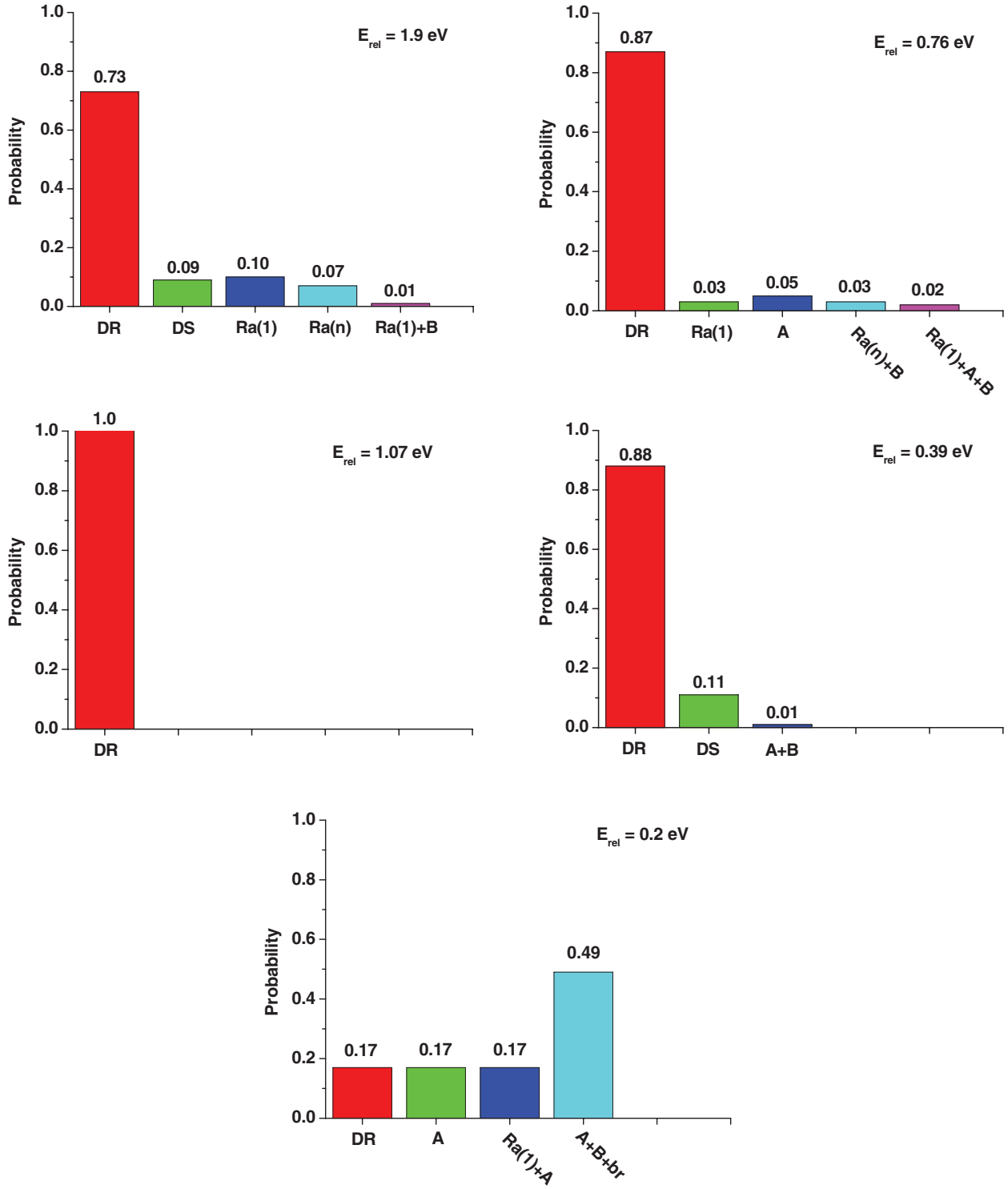

FIG. 5. Probability of the individual reaction mechanisms for E_{rel} of 0.2–1.9 eV and $T_v/T_r = 360$ K/75 K calculated at the MP2(fc)/ECP/d level of theory. DR, direct rebound; DS, direct stripping; Ra (1) and Ra (n), roundabout with one and multiple CH_3 rotations, respectively; A, Cl^-–CH_3I; B, $ClCH_3$–I^-; br, barrier-recrossing. Ra, A, B, and br are indirect mechanisms. The trajectory results are properly weighted by b and $P_r(b)$ the reaction probability versus b.

to 1.07 eV. At $E_{rel} = 0.76$ eV there are 5 direct rebound and 1 roundabout trajectory, coupled with barrier recrossing and formation of both the pre- and post-reaction complexes. The dynamics changes in going from E_{rel} of 0.39 to 0.20 eV as found for the above $b > 0$. At $E_{rel} = 0.39$ eV, with $b = 0$, there are 5 direct rebound, 1 roundabout, and 1 trajectory with both pre- and post-reaction complex formation and barrier recrossing. In contrast, at $E_{rel} = 0.20$ eV there are no direct rebound trajectories and, instead, 3 trajectories which form the pre-reaction complex, 1 roundabout trajectory, and 2

RIGHTSLINK

TABLE I. Average fractions of product energy partitioning for $Cl^- + CH_3I \rightarrow ClCH_3 + I^-$ reactive scattering at the MP2(fc)/ECP/d level of theory.[a,b]

	f_{rot}'	f_{vib}'	f_{trans}'	f_{int}'
		1.9 eV		
Direct rebound	0.04 ± 0.02	0.25 ± 0.03	0.71 ± 0.03	0.29 ± 0.03
Direct stripping	0.03	0.30	0.67	0.33
Indirect	0.21 ± 0.04	0.59 ± 0.05	0.20 ± 0.04	0.80 ± 0.04
Total	0.07 ± 0.03	0.31 ± 0.04	0.62 ± 0.05	0.38 ± 0.05
Expt.[c]	...	...	...	40%
PST[d]	...	...	...	88%
		1.07 eV		
Direct rebound	0.004 ± 0.001	0.23 ± 0.01	0.76 ± 0.01	0.24 ± 0.01
Expt.	...	...	...	25%
		0.76 eV		
Direct rebound	0.02 ± 0.01	0.37 ± 0.06	0.61 ± 0.07	0.39 ± 0.07
Indirect	0.09 ± 0.07	0.83 ± 0.02	0.08 ± 0.05	0.92 ± 0.05
Total	0.03 ± 0.01	0.43 ± 0.07	0.54 ± 0.08	0.46 ± 0.08
Expt.	...	...	...	40%
		0.39 eV		
Direct rebound	0.03 ± 0.01	0.48 ± 0.04	0.49 ± 0.04	0.51 ± 0.04
Direct stripping	0.005	0.48	0.51	0.49
Indirect	0.17	0.72	0.11	0.89
Total	0.03 ± 0.01	0.48 ± 0.03	0.49 ± 0.04	0.51 ± 0.04
Expt.	...	...	...	84%
		0.2 eV		
Direct rebound	0.03	0.77	0.20	0.80
Indirect	0.02 ± 0.01	0.86 ± 0.04	0.12 ± 0.04	0.88 ± 0.04
Total	0.02 ± 0.01	0.84 ± 0.03	0.14 ± 0.03	0.86 ± 0.03
Expt.	...	...	...	...

[a]The vibrational and rotational temperatures of CH_3I are 360 and 75 K, respectively.[27] The *f*'s are fractions of energy partitioning for rotational, vibrational, relative translational, and internal energy.
[b]Trajectories were averaged over all impact parameters (*b*) and properly weighted by *b* and the reaction probability versus *b*.
[c]Experimental value in Ref. 27.
[d]The loose transition state model of PST; Ref. 55.

trajectories with the roundabout coupled to pre-reaction complex formation.

The very low reaction probability (Figure 3) and the long lifetime of the collision intermediate make it difficult to obtain more reactive trajectories with MP2 for $E_{rel} = 0.20$ eV. However, as presented in Sec. IV, significantly more reactive trajectories were obtained with DFT/BhandH theory for this energy and BhandH gives similar atomic-level mechanisms as found with MP2.

B. Product energies

To assist in verifying the above atomic-level reaction mechanisms, the partitioning of available product energy to CH_3Cl vibration and rotation and $CH_3Cl + I^-$ relative translation, found from the simulations, may be compared with the partitioning determined from the ion imaging experiments, reported in Figure 2. The simulation and experimental product energy partitionings are compared in Table I. From the simulations the overall fraction partitioned to internal excitation of CH_3Cl (i.e., vibration and rotation) is 0.38 ± 0.05, 0.24 ± 0.01, 0.46 ± 0.08, 0.51 ± 0.04, and 0.86 ± 0.03 for E_{rel} of 1.9, 1.07, 0.76, 0.39, and 0.20 eV, respectively. At E_{rel} of 1.07 eV a minimum is found in the fraction partitioned to CH_3Cl internal excitation, a finding in very good agreement with experiment.[27,28] Table I indicates that the simulations agree well with the experiments for partitioning to CH_3Cl internal excitation except at E_{rel} of 0.39 eV, for which the simulation's fraction is 0.51 ± 0.04 and substantially smaller than the experimental fraction of 0.84. However, when E_{rel} is slightly decreased to 0.20 eV the simulation gives a much higher partitioning of 0.86 ± 0.03 to CH_3Cl internal energy, which agrees with experiment at E_{rel} of 0.39 eV. This result illustrates the extraordinary sensitivity of the product energy partitioning to the collision energy for low collision energies and suggests there may be a significant distribution of collision energies for the experiment at the low E_{rel} of 0.39 eV. The strikingly different product energy partitioning at E_{rel} of 0.39 and 0.20 eV is in accord with the much different reaction mechanisms at these two collision energies. The reaction dynamics at low E_{rel} are discussed in more detail below in Sec. IV.

As shown in Table I, the different atomic-level mechanisms observed in the simulations give different product energy partitionings. For E_{rel} of 0.39–1.9 eV the indirect mechanisms partition substantially more energy into CH_3Cl internal excitation than do the direct mechanisms. However, for E_{rel} of 0.20 eV the energy partitioning for the direct and indirect mechanisms are similar. Also of interest is that the energy

RIGHTSLINK

partitioning for the direct rebound and stripping reactions is the same within statistical uncertainties. PST, which assumes that a long-lived complex dissociates directly to products, is a statistical model for calculating product energy partitioning.[55] Though the $ClCH_3$–I^- post-reaction complex is not formed, at $E_{rel} = 1.9$ eV the roundabout mechanism leads to a CH_3Cl internal energy distribution similar to the PST prediction of 88%.[27] Only for the roundabout mechanism at $E_{rel} = 1.9$ eV is a significant fraction of the product energy partitioned to rotation. The dynamics leading to the energy partitioning for the roundabout mechanism is discussed below in Sec. V.

The product energy partitioning found for $X^- + CH_3Y \rightarrow XCH_3 + Y^-$ S_N2 reactions from previous chemical dynamics simulations has been recently reviewed[20] and it is of interest to compare this earlier work with the current study. For the $F^- + CH_3I$ S_N2 reaction at 0.32 eV,[31] indirect mechanisms were found to partition more energy into product CH_3F vibration than the direct mechanisms, which is in accord with the current results for $Cl^- + CH_3I$. The overall trend for the $Cl^- + CH_3I$ reaction is for the energy partitioned to $ClCH_3 + I^-$ relative translation to increase with increase in E_{rel} and this is the result found previously for the $F^- + CH_3Cl$ and $Cl^- + CH_3Br$ reactions.[18,24]

C. Velocity scattering angle distributions

The velocity scattering angle θ between the initial and final relative velocity vectors was determined for the simulations, and the average value of the velocity scattering angle and its range of values are given in Table II at each 0.20–1.90 eV collision energy. More details of the velocity scattering angle distributions are summarized in Table S1 in the supplementary material.[56] If the scattering angle is $<90°$, there is forward scattering, and the CH_3Cl product scatters in the same direction as the initial relative velocity. For a scattering angle $>90°$, the scattering is backward with the direction of the relative velocity vector reversed.

At all collision energies the direct rebound reaction, which is important at smaller impact parameters b, displays strong backward scattering. For direct reaction there is a tendency toward forward scattering as b is increased, which is indicative of a stripping mechanism. These dynamics are similar to those found from a trajectory study of the $Cl^- + CH_3Cl$ S_N2 reaction at high reagent translational energy,[53] for which the trajectory events were direct. The trajectories for the indirect reactions have both forward and backward scattering.

The velocity scattering angle distributions determined from the ion imaging experiments are given in Figure 2, for the different E_{rel}, and the simulations are consistent with these findings. At 1.9 eV the experimental scattering is primarily in the backward direction with high relative translational energies, as observed in the simulations for the rebound mechanism. There is also a significant component in the backward direction with a much smaller translational energy, which arises from the rebound mechanism. There is a quite small scattering component in the forward direction, which the trajectories indicate arises from both direct stripping and roundabout events. There is not an isotropic component in the scattering at 1.9 eV. For both the simulations and experiments at 1.07 eV, all of the reaction is direct and the scattering is in the backward direction. At 0.76 eV the experimental scattering has a prominent backward component with a high relative translational energy and an isotropic component with a lower translational energy. The simulation gives similar scattering, with direct rebound events leading to backward scattering, and formation of the pre- and post-reaction complexes leading to the isotropic scattering. For the experiments at E_{rel} of 0.39 eV the scattering is completely isotropic and the product relative translational energy distribution agrees with that of PST theory (Figure 2).[27] The simulations at this E_{rel} are not in accord with the experiments, but the simulations at $E_{rel} = 0.20$ eV give results similar to experiment. The total scattering is quite isotropic with an average value near 90°. As discussed above, the product energy partitioning for this lower E_{rel} also matches experiment at $E_{rel} = 0.39$ eV.

D. Effect of vibrational and rotational temperatures

To compare with the above calculations for the experimental temperatures $T_v = 360$ K and $T_r = 75$ K, an additional calculation was performed with the MP2(fc)/ECP/d theory for room temperature, i.e., both T_v and T_r equal 300 K, and for $E_{rel} = 1.9$ eV. The reaction probability $P_r(b)$ for the two sets of calculations are compared in Figure 6. Changing T_v/T_r from 360/75 K to 300/300 K has a only a small effect on the reaction probability and the effect is to slightly decrease $P_r(b)$. Figure 7 shows the fractions of the atomic-level mechanisms for $T_v/T_r = 300/300$ K and E_{rel} of 1.9 eV. By comparison with

TABLE II. Average and range of values for the velocity scattering angle at the MP2(fc)/ECP/d level of theory.[a,b]

E_{rel} (eV)	Direct rebound	Direct stripping	Indirect	Total
1.9	134 (116–160)	85	90 (17–158)	121 (17–160)
1.07	152 (128–167)	...	...	152 (128–167)
0.76	142 (126–159)	...	68 (4–125)	133 (4–159)
0.39	128 (111–162)	88	25	122 (25–162)
0.2	159	...	102 (55–145)	113 (55–159)

[a]Scattering angles in degree between the initial (i) and final (f), relative velocity (v). The range of values is given in parentheses. The vibrational and rotational temperatures of CH_3I are 360 and 75 K, respectively.[27]

[b]Trajectories were averaged over all impact parameters (b) and properly weighted by b and the reaction probability versus b.

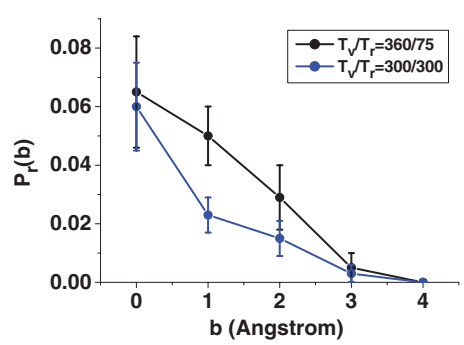

FIG. 6. Comparison of $T_v/T_r = 360/75$ K and $T_v/T_r = 300/300$ K reaction probability $P_r(b)$ for E_{rel} of 1.9 eV as given by MP2(fc)/ECP/d theory.

RIGHTSLINK

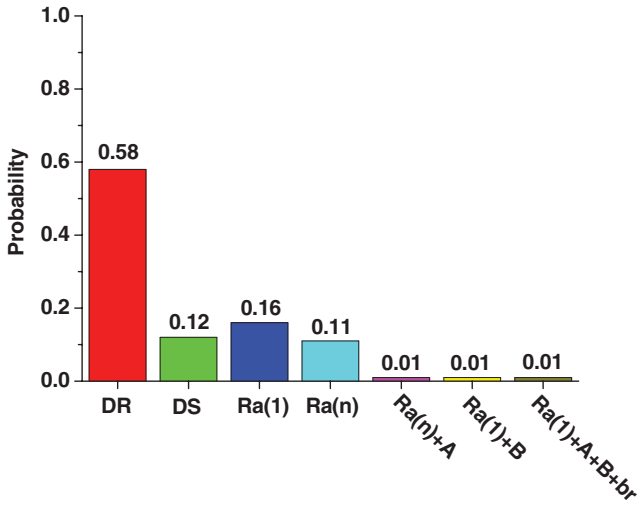

FIG. 7. Probability of the individual reaction mechanisms for E_{rel} of 1.9 eV and T_v/T_r = 300/300 K as given by MP2(fc)/ECP/d theory. The representations for the individual mechanisms are the same as those in Figure 5. The trajectory results are properly weighted by b and the reaction probability versus b.

that for T_v/T_r = 360/75 K and the same E_{rel} in Figure 5, the principal reaction mechanism is direct rebound for both sets of temperatures and the indirect reaction occurs mainly by a roundabout mechanism. The fraction of the roundabout mechanism with one or multiple CH_3 rotations increases from 17% to 27% as T_v/T_r is changed from 360/75 K to 300/300 K.

The product energy partitioning for E_{rel} of 1.9 eV and T_v/T_r = 300/300 K is given in Table III, which may be compared with those in Table I for E_{rel} of 1.9 eV and T_v/T_r = 360/75 K. The major difference, between the two sets of calculations, is in the energy partitioned to rotation and relative translation. Overall, the rotational energy is higher and the relative translational energy lower for total reaction and the individual reaction mechanisms at T_v/T_r = 300/300 K. Temperature has only a small effect on the CH_3Cl vibrational energy. The overall fraction partitioned to internal excitation of CH_3Cl is 0.48 at T_v/T_r = 300/300 K and ~25% higher than the value at T_v/T_r = 360/75 K, which results from the higher rotational energy at T_v/T_r = 300/300 K. The scattering angle properties for E_{rel} of 1.9 eV and T_v/T_r = 300/300 K are given in Table S2 in the supplementary material[56] and are statistically the same as those for T_v/T_r = 360/75 K.

TABLE III. Average fractions of product energy partitioning for E_{rel} of 1.9 eV and T_v/T_r = 300/300 K at MP2(fc)/ECP/d level of theory.[a]

	f_{rot}'	f_{vib}'	f_{trans}'	f_{int}'
Direct rebound	0.11 ± 0.05	0.22 ± 0.02	0.67 ± 0.06	0.33 ± 0.06
Direct stripping	0.06	0.21	0.73	0.27
Indirect	0.27 ± 0.05	0.56 ± 0.08	0.17 ± 0.05	0.83 ± 0.05
Total	0.15 ± 0.04	0.33 ± 0.05	0.52 ± 0.08	0.48 ± 0.08
Expt.[b]	...	...	...	40%

[a]The f's are fractions of energy partitioning for rotational, vibrational, relative translational, and internal energy. Trajectories were averaged over all impact parameters (b) and properly weighted by b and the reaction probability versus b.
[b]For experiment the collision energy is 1.9 eV, and the vibrational and rotational temperatures of CH_3I are 360 and 75 K, respectively.[27]

In summarizing the differences between the simulations for T_v/T_r of 300/300 K as compared to those for 360/75 K, the former gives rise to more rotational energy in the CH_3Cl product and a larger fraction of roundabout trajectories. Apparently this arises from the larger reactant rotational energy for the T_v/T_r = 300/300 K simulation.

IV. COMPARISON BETWEEN MP2 AND DFT TRAJECTORIES

To further investigate the above dynamics obtained with MP2 theory at the low collision energies of 0.39 and 0.20 eV, a direct dynamics simulation was also performed using the BhandH/ECP/d DFT method. In previous work,[32] many different DFT functionals were evaluated to characterize properties of stationary points on the $Cl^- + CH_3I \rightarrow ClCH_3 + I^-$ PES and the BhandH/ECP/d method was found to give the best agreement with the benchmark CCSD(T)/CBS energies, with the largest difference of 0.7 kcal/mol for both the Cl^-–CH_3I pre-reaction minimum and $[Cl–CH_3–I]^-$ TS.

The reaction probability $P_r(b)$ as a function of b for both MP2 and BhandH is plotted in Figure 8 for the calculations at E_{rel} of 0.39 and 0.20 eV. For both E_{rel} values BhandH gives the higher $P_r(b)$, which is consistent with the lower BhandH central barrier of −6.4 kcal/mol as compared to the MP2 value of −4.0 kcal/mol (see Figure 1).[32] The BhandH fractions of different reaction mechanisms, for E_{rel} of 0.39 and 0.20 eV, are shown in Figure 9. There are 51 and 28 reactive trajectories with $b > 0$ for E_{rel} of 0.39 and 0.20 eV, respectively, and they are properly weighted by the impact parameters to

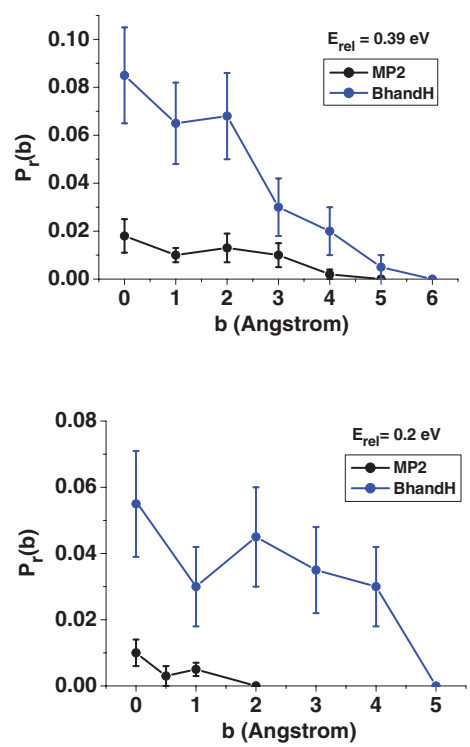

FIG. 8. Comparison of reaction probability versus impact parameter, $P_r(b)$, for MP2 and BhandH calculations with the ECP/d basis set. Calculations are for E_{rel} of 0.20 and 0.39 eV and T_v/T_r = 360 K/75 K.

RIGHTSLINK

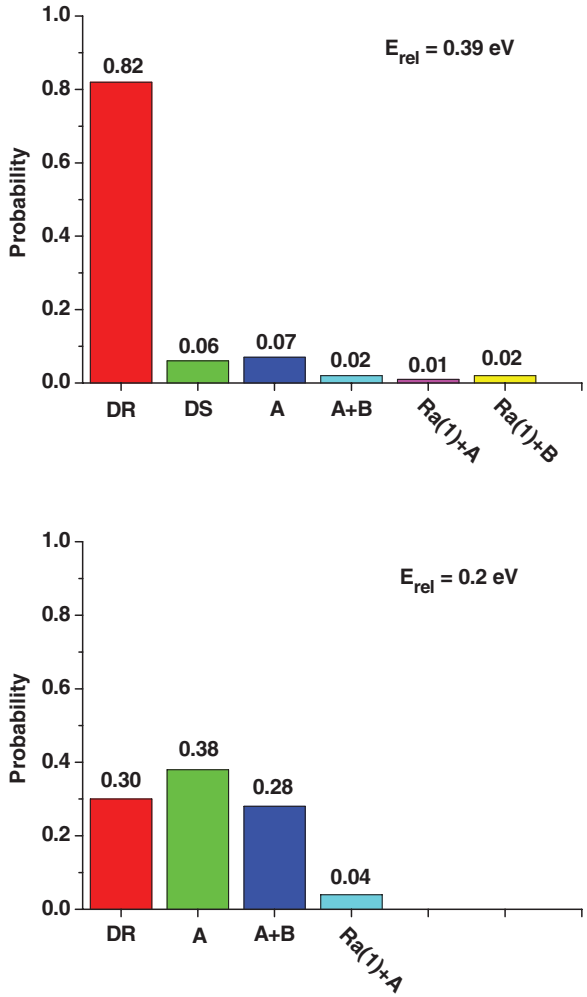

FIG. 9. Same as Figure 4 but for the BhandH/ECP/d calculations at E_{rel} of 0.20 and 0.39 eV with $T_v/T_r = 360$ K/75 K.

obtain the fractions in Figure 9. With $b = 0$ included the total number of reactive trajectories for these respective E_{rel} are 68 and 39. Comparing these results with those for MP2 in Figure 5 shows that, overall, the BhandH and MP2 atomic-level mechanisms are very similar. For E_{rel} of 0.20 eV the direct fraction is 0.17 ± 0.03 and 0.30 ± 0.03 for the MP2 and BhandH calculations, respectively. For $E_{rel} = 0.39$ eV the results are significantly different from what is found at $E_{rel} = 0.20$ eV, and the respective direct fraction is 0.99 ± 0.10 and 0.88 ± 0.09 for MP2 and BhandH. At $E_{rel} = 0.39$ eV the indirect mechanisms are more important contributors to reaction for the BhandH calculations than for the calculations using MP2. For both the MP2 and BhandH calculations, A and A + B events are important for the indirect mechanisms at $E_{rel} = 0.20$ eV. However, at this energy, roundabout events are important with MP2 but not with BhandH. The intermediate lifetimes for the BhandH calculations range from 1 to 7 ps for the indirect mechanisms and are similar to those for the MP2 calculations (see Sec. III A).

The $b = 0$ BhandH results show much different dynamics between E_{rel} of 0.39 and 0.20 eV, as discussed above and shown in Figure 9. At 0.39 eV all the seventeen $b = 0$ trajectories are direct rebound. At 0.20 eV 4 of the trajectories are direct rebound and 7 are indirect. The latter involve pre-reaction complex formation, formation of both the pre- and post-reaction complexes, and coupling of the roundabout with the pre-reaction complex.

TABLE IV. Average fractions of product energy partitioning at BhandH/ECP/d level of theory.[a,b]

	f_{rot}'	f_{vib}'	f_{trans}'	f_{int}'
		0.39 eV		
Direct rebound	0.04 ± 0.01	0.38 ± 0.04	0.58 ± 0.04	0.42 ± 0.04
Direct stripping	0.02	0.33	0.65	0.35
Indirect	0.05 ± 0.01	0.89 ± 0.01	0.06 ± 0.01	0.94 ± 0.01
Total	0.04 ± 0.01	0.44 ± 0.06	0.52 ± 0.07	0.48 ± 0.07
Expt.[c]	...	...	...	84%
		0.20 eV		
Direct rebound	0.02 ± 0.01	0.58 ± 0.09	0.40 ± 0.08	0.60 ± 0.08
Indirect	0.07 ± 0.02	0.81 ± 0.05	0.12 ± 0.04	0.88 ± 0.04
Total	0.06 ± 0.02	0.74 ± 0.07	0.20 ± 0.07	0.80 ± 0.07
Expt.	...	...	...	...

[a]The vibrational and rotational temperatures of CH_3I are 360 and 75 K, respectively.[27] The f's are fractions of energy partitioning for rotational, vibrational, relative translational, and internal energy.
[b]Trajectories were averaged over all impact parameters (b) and properly weighted by b and the reaction probability versus b.
[c]Experimental value in Ref. 27.

The product energy partitionings for the BhandH simulations are listed in Table IV and may be compared with those in Table I for the MP2 simulations. The overall fraction partitioned to CH_3Cl internal excitation is in quite good agreement for the MP2 and BhandH calculations. The respective MP2 and BhandH fractions are 0.51 ± 0.04 and 0.48 ± 0.07 at 0.39 eV and 0.86 ± 0.03 and 0.80 ± 0.07 at 0.20 eV. At the level of the individual atomic-level mechanisms, there are both similarities and differences in the MP2 and BhandH product energy partitioning. At 0.39 eV the direct rebound and direct stripping mechanisms have similar product energy partitionings for both BhandH and MP2, and at 0.20 eV the only direct mechanism is rebound for both MP2 and BhandH. However, comparing the results in Tables I and IV shows that BhandH partitions a larger fraction to product translation for the direct reactions. On the other hand, The product energy partitioning for the indirect mechanisms are similar for MP2 and BhandH at $E_{rel} = 0.20$ eV. The BhandH and MP2 internal energy fractions at 0.39 eV are substantially smaller than the 84% found in the experiments. But the fraction at 0.20 eV from the simulations is in good agreement with experiment at 0.39 eV. In summary, BhandH partitions more energy to product translation for the direct mechanisms, but the total product energy partitionings are quite similar for the MP2 and BhandH simulations.

BhandH and MP2 give similar scattering angle distributions at both the 0.39 and 0.20 eV collision energies. Details of these distributions are given in Table II and Table S1 in the supplementary material[56] for MP2, and in Table S3 in the supplementary material[56] for BhandH. The experimental velocity scattering angle distribution at $E_{rel} = 0.39$ eV is isotropic (Figure 2), consistent with indirect reaction and a long-lived intermediate. The simulation velocity scattering angle distributions for $E_{rel} = 0.39$ eV do not agree with experiment, but

RIGHTSLINK

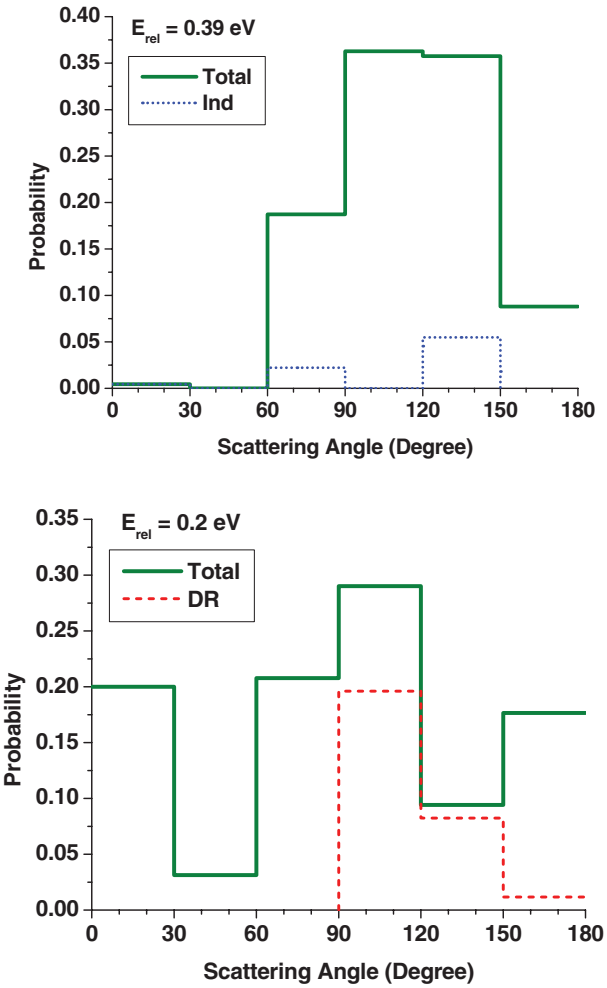

FIG. 10. Velocity scattering angle distributions for E_{rel} of 0.20 and 0.39 eV, formed by combining the MP2 and BhandH results at each of these energies.

the simulations at $E_{rel} = 0.20$ eV do. Though there is a 17%–30% direct component in the simulations at 0.20 eV, both the MP2 and BhandH velocity scattering angle distributions are broad and quite isotropic, with average values near 90°. Figure 10 compares the velocity scattering angle distributions for E_{rel} of 0.20 and 0.39 eV, with those for MP2 and BhandH combined. The difference in the scattering at these two energies is striking. The scattering is primarily backward at 0.39 eV, but isotropic at 0.20 eV.

V. ROUNDABOUT MECHANISM

Statistical models for product energy partitioning assume that a long-lived $ClCH_3$–I^- post-reaction complex is formed with complete randomization of its vibrational energy.[25] Different statistical models have been proposed, depending on the assumed dynamics as the products separate.[57–59] The loose transition state (TS) model of PST was used here, for which the TS is placed in the product asymptotic limit.[25,55] As summarized in Table I, PST predicts a much higher 88% partitioning to the CH_3Cl internal energy than experiment at E_{rel} of 1.9 eV. In contrast, the PST prediction is in approximate agreement with that of 0.80 ± 0.04 for the indirect roundabout

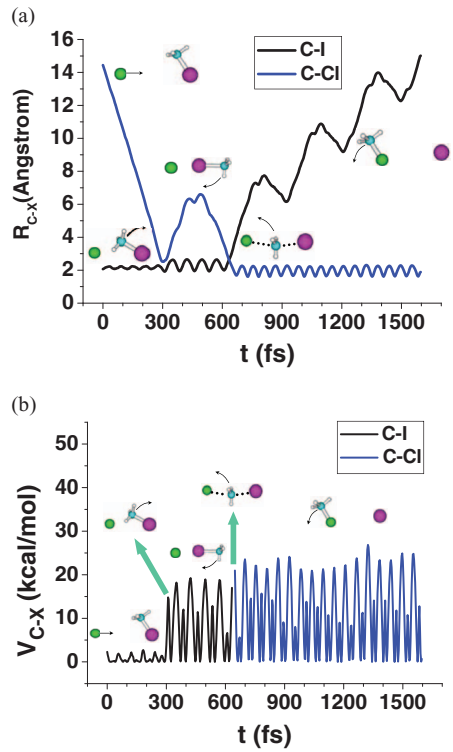

FIG. 11. (a) C-X (X = I and Cl) distances versus time for a representative roundabout trajectory involving a single CH_3 rotation. (b) The C-X (X = I and Cl) bond stretch potential energies as a function of time for the roundabout trajectory in (a).

trajectories. This agreement occurs even though the $ClCH_3$–I^- post-reaction complex is not formed in the roundabout mechanism as assumed by PST.

A detailed analysis was made to investigate why the dynamics of the roundabout mechanism, gives product energy partitioning similar to that of PST. Plotted in Figure 11(a) are the C-X (X = I and Cl) distances versus time for a representative trajectory of the roundabout reaction at E_{rel} of 1.9 eV, that proceeds via one CH_3 rotation. At ∼300 fs there is an initial collision between Cl^- and the CH_3 group, which excites the C-I stretch vibration and causes CH_3 to rotate about the massive I atom. The latter is identified by the increase and subsequent decrease of C-Cl distance. After one CH_3 rotation S_N2 substitution occurs, forming a C-Cl bond with substantial vibrational excitation.

The energy transfer dynamics from reactants to products was studied by determining the C-I and C-Cl bond stretch energies and the CH_3I and CH_3Cl rotational energies versus time for all the roundabout trajectories at E_{rel} of 1.9 eV. The C-I potential energy curve was taken as that for the Cl^-–CH_3-I pre-reaction complex and the C-Cl potential energy curve as that for the Cl-CH_3–I^- post-reaction complex. These potential curves were calculated at the MP2(fc)/ECP/d theory, used for the simulations, and then fit by the Morse function $V(r) = D_e[1\text{-}e^{-\beta(\text{r-re})}]^2$ as shown in Figure S1 in the supplementary material.[56] These curves are nearly identical to those for the CH_3-I and Cl-CH_3 reactant and product, respectively, and were used to determine the potential energies in the C-I and C-Cl bonds versus

RIGHTSLINK

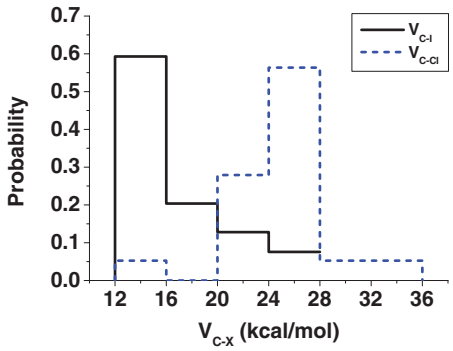

FIG. 12. Distributions of the C-X (X = I and Cl) bond stretch potential energies for all the roundabout trajectories at $E_{rel} = 1.9$ eV. The C-I bond stretch energy is the energy after the initial reactant collision and the C-Cl bond stretch energy is that for the CH_3Cl product.

time. The energies in these bonds versus time, for the representative roundabout trajectory in Figure 11(a), are plotted in Figure 11(b). The C-I bond stretch energy distribution after the initial collision of reactants and the product C-Cl bond stretch energy distribution for all the roundabout trajectories at $E_{rel} = 1.9$ eV are depicted in Figure 12. The average energies of these distributions are used for the following analyses.

During the initial collision of the reactants at ~300 fs there is 55.4 kcal/mol of energy available for transfer, i.e., the 43.8 kcal/mol (1.9 eV) collision energy plus the 11.6 kcal/mol potential energy release in accessing the Cl^-–CH_3I potential energy minimum (Figure 1). Of this energy ~16.5 kcal/mol is transferred to the C-I bond, an amount higher than the potential energy barrier of 7.6 kcal/mol in going from the Cl^-–CH_3I complex to the $[Cl–CH_3–I]^-$ TS (Figure 1). In addition, 30.0 kcal/mol is transferred to CH_3I rotation, with CH_3 rotating about the massive I-atom. After one CH_3-rotation Cl^- again collides with CH_3 and now, with the C-I bond excited, S_N2 substitution occurs. As shown in Figure 11, the excited C-I bond of the reactants leads to lengthened C-I and C-Cl bonds at the TS, resulting in a short C-Cl distance at the first inner point of the C-Cl bond stretch and a large product C-Cl stretch energy of ~26.0 kcal/mol. The large CH_3 angular velocity about the I atom in the entrance channel, results in a high rotational angular momentum and rotational energy of 12.0 kcal/mol for CH_3Cl in the exit channel. The high vibrational and rotational energies of the excited CH_3I reactant are transferred to the CH_3Cl product.

The total available energy is preferentially partitioned to internal modes (i.e., vibration and rotation) of the CH_3Cl product for the roundabout trajectories. For all the roundabout trajectories at $E_{rel} = 1.9$ eV the CH_3Cl internal modes receive ~80% of the available energy, close to the PST prediction of 88%. Approximately 60% of the energy transfer for the trajectories is to CH_3Cl vibration and ~20% to CH_3Cl rotation. Of this transfer to vibration, ~78% is to the C-Cl bond.

VI. SUMMARY

These combined experimental and direct dynamics simulation results provide a detailed understanding of the atomic-level dynamics for the gas-phase $Cl^- + CH_3I \rightarrow ClCH_3 + I^-$ S_N2 nucleophilic substitution reaction. Simulations at the MP2(fc)/ECP/d level of theory are in very good agreement with the experimental product energy partitioning and velocity scattering angles for the collision energies E_{rel} of 0.76, 1.07, and 1.9 eV. For these energies the reaction is dominated by direct rebound reaction with backward scattering. There is a small direct stripping component with forward scattering. The indirect component of the reaction consists of the roundabout mechanism, formation of the pre- and post-reaction ion-dipole complexes, and barrier recrossing events. The roundabout events do not scatter isotropically, but the latter three do. Complex formation is important at 0.76 eV, but unimportant at the higher E_{rel}. No indirect reaction is seen in the trajectories at 1.07 eV, but it becomes important again at 1.9 eV via another pathway the roundabout mechanism. Thus, complex formation is a low collision energy indirect mechanism, while the roundabout mechanism becomes an important indirect pathway at high collision energy.

For E_{rel} of 0.76, 1.07, and 1.9 eV the product energy partitioning is primarily to relative translation for the direct reactions, but to CH_3Cl internal energy for the indirect reactions. The roundabout mechanism transfers substantial energy to CH_3Cl rotation and measuring this experimentally would be a diagnostic for the roundabout mechanism. For the other indirect mechanisms the energy partitioning is primarily to CH_3Cl vibration.

For the experiments at the lowest collision energy of 0.39 eV the product energy partitioning is statistical, agreeing with PST, and the scattering is isotropic. Both are indicative of an indirect reaction, with an intermediate, and the PST model further assumes that a long-lived $ClCH_3$–I^- post-reaction complex is formed with statistical redistribution of its energy and a RRKM lifetime.[25] The MP2 simulations at this E_{rel} do not reproduce experiment and instead give dynamics similar to those at the higher collision energies. To ascertain if this disagreement with experiment results from inaccuracies in the MP2 PES, simulations were also performed with the DFT/BhandH/ECP/d PES. A previous study has shown that the latter level of theory gives PES energies in excellent agreement with those obtained using CCSD(T) theory.[32] BhandH was found to also give dynamics in disagreement with experiment, similar to the MP2 dynamics. However, by slightly decreasing E_{rel} to 0.20 eV, both MP2 and BhandH give product energy partitioning and velocity scattering distributions in agreement with the experiment at $E_{rel} = 0.39$ eV. At both E_{rel} of 0.39 and 0.20 eV the MP2 and BhandH simulations give similar reaction dynamics, and there is a sharp transition in the dominant reaction mechanism from direct to indirect as E_{rel} is lowered from 0.39 to 0.20 eV. It is noteworthy that, as for the $Cl^- + CH_3I$ reaction, there is a sharp transition between indirect and direct mechanisms for the $Cl^- + CH_3Br$ reaction at an E_{rel} of ~0.3–0.6 eV.[24,60]

The similarity in the reaction dynamics for the MP2 and BhandH simulations suggests that if there is a shortcoming in the simulations it resides in the quasiclassical trajectory calculation. It is possible that some of the zero-point energy within CH_3I is transferred to its C-I bond, as Cl^- and CH_3I approach, promoting a direct reaction.[17,18] Another possibility is that the reactants cross the central barrier without zero

RIGHTSLINK

point energy in the degrees of freedom orthogonal to the reaction coordinate.[61] These are interesting questions to address in future studies. It would be particularly interesting to "map out" the changes in the reaction mechanisms as the collision energy is varied between 0.39 and 0.20 eV. Experimentally, this will be facilitated using cold trapped ions as reactants for reactive scattering experiments,[62] which will allow for a better resolution of the relative collision energy.

A simulation was performed at $E_{rel} = 1.9$ eV with a vibrational and rotational temperature of 300 K, to compare with the experiments and simulations at $T_v/T_r = 360$ K/75 K. It was found that both the partitioning of energy to CH_3Cl rotation and the fraction of the roundabout mechanism increase when T_v/T_r is changed from 360 K/75 K to 300 K/300 K. Presumably this is because of the increase in the reactant rotational energy for the $T_v/T_r = 300$ K/300 K simulation.

In the roundabout mechanism a large fraction of the reactants' collision energy is transferred to C-I stretch vibration and rotation of CH_3 about the massive I atom. After one or multiple rotations of the CH_3-group, the S_N2 reaction occurs forming CH_3Cl with significant rotational energy and an excited C-Cl bond. Thus, CH_3Cl has a high internal excitation, resulting in a product relative translational energy in approximate agreement with PST.

In concluding, two interesting changes in the $Cl^- + CH_3I$ S_N2 reaction dynamics were identified as the collision energy is varied. At low collision energy, there is a transition from a dominant indirect reaction with pre- and post-reaction complex formation to a dominant direct reaction occurring via the rebound mechanism. As the collision energy is further increased, the indirect reaction is completely suppressed and there is only direct reaction. With further increase in the collision energy indirect reaction again occurs, but via the roundabout mechanism. Increasing the reactant CH_3I rotational energy increases the fraction of the reaction occurring via the roundabout mechanism. In the future it would be of interest to further investigate the effect of CH_3I rotation on the reaction dynamics, as well as CH_3I vibration, particularly the C-I stretch.

ACKNOWLEDGMENTS

The calculations reported here are based upon work supported by the National Science Foundation under Grant Nos. CHE-0615321 and CHE-0957521, and the Robert A. Welch Foundation under Grant No. D-0005. Support was also provided by the High-Performance Computing Center (HPCC) at Texas Tech University, under the direction of Philip W. Smith, the Texas Advanced Computing Center (TACC) at the University of Texas at Austin, and the Environmental Molecular Sciences Laboratory (EMSL) at the Pacific Northwest National Laboratory (PNNL). The experimental work was supported by the Deutsche Forschungsgemeinschaft (DFG) under Grant No. WE 2592/3-2. Dr. Li Yang is acknowledged for important discussions concerning the direct dynamics simulations.

[1] C. A. Lieder and J. I. Brauman, J. Am. Chem. Soc. **96**, 4029 (1974).
[2] J. I. Brauman, W. N. Olmstead, and C. A. Lieder, J. Am. Chem. Soc. **96**, 4030 (1974).
[3] W. N. Olmstead and J. I. Brauman, J Am. Chem. Soc. **99**, 4219 (1977).
[4] S. Shaik, A. Ioffe, A. C. Reddy, and A. Pross, J. Am. Chem. Soc. **116**, 262 (1994).
[5] M. L. Chabinyc, S. L. Craig, C. K. Regan, and J. I. Brauman, Science **279**, 1982 (1998).
[6] L. A. Angel and K. M. Ervin, J. Phys. Chem. A **108**, 9827 (2004).
[7] S. T. Graul and M. T. Bowers, J. Am. Chem. Soc. **116**, 3875 (1994).
[8] S. T. Graul and M. T. Bowers, J. Am. Chem. Soc. **113**, 9696 (1991).
[9] A. A. Viggiano, R. A. Morris, J. S. Paschkewitz, and J. F. Paulson, J. Am. Chem. Soc. **114**, 10477 (1992).
[10] R. Wester, A. E. Bragg, A. V. Davis, and D. M. Neumark, J. Chem. Phys. **119**, 10032 (2003).
[11] C. Li, P. Ross, J. E. Zsulejko, and T. B. McMahon, J. Am. Chem. Soc. **118**, 9360 (1996).
[12] D. S. Tonner and T. B. McMahon, J. Am. Chem. Soc. **122**, 8783 (2000).
[13] J. Mikosch, R. Otto, S. Trippel, C. Eichhorn, M. Weidemüller, and R. Wester, J. Phys. Chem. A **112**, 10448 (2008).
[14] S. L. Craig and J. I. Brauman, J. Phys. Chem. A **101**, 4745 (1997).
[15] H. Wang and W. L. Hase, J. Am. Chem. Soc. **117**, 9347 (1995).
[16] W. L. Hase, Science **266**, 998 (1994).
[17] S. R. Vande Linde and W. L. Hase, J. Chem. Phys. **93**, 7962 (1990).
[18] S. R. Vande Linde and W. L. Hase, J. Am. Chem. Soc. **111**, 2349 (1989).
[19] H. Wang, G. H. Peslherbe, and W. L. Hase, J. Am. Chem. Soc. **116**, 9644 (1994).
[20] P. Manikandan, J.-X. Zhang, and W. L. Hase, J. Phys. Chem. A **116**, 3061 (2012).
[21] G. Li and W. L. Hase, J. Am. Chem. Soc. **121**, 7124 (1999).
[22] L. Sun, W. L. Hase, and K. Song, J. Am. Chem. Soc. **123**, 5753 (2001).
[23] L. Sun, K. Song, and W. L. Hase, Science **296**, 875 (2002).
[24] Y. Wang, W. L. Hase, and H. Wang, J. Chem. Phys. **118**, 2688 (2003).
[25] T. Baer and W. L. Hase, *Unimolecular Reaction Dynamics Theory and Experiments* (Oxford, New York, 1996).
[26] S. Glasstone, K. J. Laidler, and H. Eyring, *The Theory of Rate Processes* (McGraw-Hill, New York, 1941).
[27] J. Mikosch, S. Trippel, C. Eichhorn, R. Otto, U. Lourderaj, J.-X. Zhang, W. L. Hase, M. Weidemüller, and R. Wester, Science **319**, 183 (2008).
[28] J. Mikosch, "Dynamics of anion-molecule reactions at low energy," Ph.D. dissertation (Physikalisches Institut, Universität Freiburg, Germany, 2007).
[29] G. H. Peslherbe, H. Wang, and W. L. Hase, Adv. Chem. Phys. **105**, 171 (1999).
[30] L. Sun and W. L. Hase, Rev. Comput. Chem. **19**, 79 (2003).
[31] J.-X. Zhang, J. Mikosch, S. Trippel, R. Otto, M. Weidemüller, R. Wester, and W. L. Hase, J. Phys. Chem. Lett. **1**, 2747 (2010).
[32] J.-X. Zhang, U. Lourderaj, S. V. Addepalli, W. A. de Jong, and W. L. Hase, J. Phys. Chem. A **113**, 1976 (2009).
[33] W. J. Hehre, L. Radom, P. v. R. Schleyer, and J. A. Pople, *Ab Initio Molecular Orbital Theory* (Wiley, New York, 1986).
[34] T. H. Dunning, Jr., J. Chem. Phys. **90**, 1007 (1989).
[35] W. R. Wadt and P. J. Hay, J. Chem. Phys. **82**, 284 (1985).
[36] W.-P. Hu and D. G. Truhlar, J. Am. Chem. Soc. **117**, 10726 (1995).
[37] A. D. Becke, J. Chem. Phys. **98**, 1372 (1993).
[38] M. Swart, M. Solà, and F. M. Bickelhaupt, J. Comput. Chem. **28**, 1551 (2007).
[39] M. Grüning, O. Gritsenko, and E. J. Baerends, J. Phys. Chem. A **108**, 4459 (2004).
[40] O. V. Gritsenko, B. Ensing, P. R. T. Schipper, and E. J. Baerends, J. Phys. Chem. A **104**, 8558 (2000).
[41] A. P. Bento, M. Solà, and F. M. Bickelhaupt, J. Comput. Chem. **26**, 1497 (2005).
[42] M. Swart, A. W. Ehlers, and K. Lammertsma, Mol. Phys. **102**, 2467 (2004).
[43] J. M. Gonzales, R. S. Cox III, S. T. Brown, W. D. Allen, and H. F. Schaefer III, J. Phys. Chem. A **105**, 11327 (2001).
[44] B. L. Kormos and C. J. Cramer, J. Phys. Org. Chem. **15**, 712 (2002).
[45] J. Poater, M. Solà, M. Duran, and J. Robles, Phys. Chem. Chem. Phys. **4**, 722 (2002).
[46] Y. Zhao, N. González-García, and D. G. Truhlar, J. Phys. Chem. A **109**, 2012 (2005).
[47] K. Raghavachari, G. W. Trucks, J. A. Pople, and M. Head-Gordon, Chem. Phys. Lett. **157**, 479 (1989).
[48] W. L. Hase, R. J. Duchovic, X. Hu, A. Komornicki, K. F. Lim, D. H. Lu, G. H. Peslherbe, S. R. Swamy, S. R. Vande Linde, A. Varandas *et al.*, Quantum Chemistry Program Exchange (QCPE) Bulletin **16**, 671 (1996).
[49] X. Hu, W. L. Hase, and T. Pirraglia, J. Comput. Chem. **12**, 1014 (1991).

RIGHTSLINK

[50]E. J. Bylaska, W. A. de Jong, N. Govind, K. Kowalski, T. P. Straatsma, M. Valiev, D. Wang, E. Apra, T. L. Windus, J. Hammond *et al.*, "NWChem, A Computational Chemistry Package for Parallel Computers, Version 5.1" (2007), Pacific Northwest National Laboratory, Richland, Washington 99352-0999, USA.
[51]R. A. Kendall, E. Apra, D. E. Bernholdt, E. J. Bylaska, M. Dupuis, G. I. Fann, R. J. Harrison, J. Ju, J. A. Nichols, J. Nieplocha *et al.*, Comput. Phys. Commun. **128**, 260 (2000).
[52]J. Mikosch, J.-X. Zhang, S. Trippel, C. Eichhorn, R. Otto, R. Sun, W. A. de Jong, M. Weidemüller, W. L. Hase, and R. Wester, "Indirect dynamics in a highly exoergic substitution reaction," J. Am. Chem. Soc. (published online).
[53]D. J. Mann and W. L. Hase, J. Phys. Chem. A **102**, 6208 (1998).
[54]Y. J. Cho, S. R. Vande Linde, L. Zhu, and W. L. Hase, J. Chem. Phys. **96**, 8275 (1992).
[55]C. E. Klots, J. Chem. Phys. **64**, 4269 (1976).
[56]See supplementary material at http://dx.doi.org/10.1063/1.4795495 for the velocity scattering angle for the MP2 and DFT/BhandH theories and different reactants' vibrational and rotational temperatures; C-X (X = I and Cl) bond energy of the reaction complexes.
[57]W. J. Chesnavich and M. T. Bowers, in *Gas Phase Ion Chemistry*, edited by M. T. Bowers (Academic, New York, 1979), Vol. 1, pp. 119–152.
[58]S. J. Klippenstein and R. A. Marcus, J. Chem. Phys. **91**, 2280 (1989).
[59]J. Troe, V. G. Ushakov, and A. A. Viggiano, Z. Phys. Chem. **219**, 699 (2005).
[60]L. A. Angel and K. M. Ervin, J. Am. Chem. Soc. **125**, 1014 (2003).
[61]K. N. Swamy and W. L. Hase, J. Phys. Chem. **87**, 4715 (1983).
[62]R. Otto, J. Brox, S. Trippel, M. Stei, T. Best, and R. Wester, Nat. Chem. **4**, 534 (2012).
[63]L. V. Gurvich, I. V. Veyts, and C. B. Alcock, *Thermodynamic Properties of Individual Substances*, 4th ed. (Hemisphere Publishing Corporation, New York, 1989), Vol. 1, Elements O, H (D, T), F, Cl, Br, I, He, Ne, Ar, Kr, Xe, Rn, S, N, P and Their Compounds, Parts 1–2.
[64]J. L. Duncan, A. Allan, and D. C. Mckean, Mol. Phys. **18**, 289 (1970).

RIGHTSLINK